Climatic dipoles drive two principal modes of North American boreal bird irruption

Courtenay Strong[a,1], Benjamin Zuckerberg[b], Julio L. Betancourt[c], and Walter D. Koenig[d]

[a]Department of Atmospheric Sciences, University of Utah, Salt Lake City, UT 84112-0110; [b]Department of Forest and Wildlife Ecology, University of Wisconsin-Madison, Madison, WI 53706-1598; [c]National Research Program, US Geological Survey, Reston, VA 20192; and [d]Cornell Lab of Ornithology and Department of Neurobiology and Behavior, Cornell University, Ithaca, NY 14850

Edited by Janet Franklin, Arizona State University, Tempe, AZ, and approved April 13, 2015 (received for review October 6, 2014)

Pine Siskins exemplify normally boreal seed-eating birds that can be sparse or absent across entire regions of North America in one year and then appear in large numbers the next. These dramatic avian "irruptions" are thought to stem from intermittent but broadly synchronous seed production (masting) in one year and meager seed crops in the next. A prevalent hypothesis is that widespread masting in the boreal forest at high latitudes is driven primarily by favorable climate during the two to three consecutive years required to initiate and mature seed crops in most conifers. Seed production is expensive for trees and is much reduced in the years following masting, driving boreal birds to search elsewhere for food and overwintering habitat. Despite this plausible logic, prior efforts to discover climate-irruption relationships have been inconclusive. Here, analysis of more than 2 million Pine Siskin observations from Project FeederWatch, a citizen science program, reveals two principal irruption modes (North-South and West-East), both of which are correlated with climate variability. The North-South irruption mode is, in part, influenced by winter harshness, but the predominant climate drivers of both modes manifest in the warm season as continental-scale pairs of oppositely signed precipitation and temperature anomalies (i.e., dipoles). The climate dipoles juxtapose favorable and unfavorable conditions for seed production and wintering habitat, motivating a push-pull paradigm to explain irruptions of Pine Siskins and possibly other boreal bird populations in North America.

avian irruption | boreal birds | climate variability | migration | masting

Avian migration is one of the most visible and well-studied phenomena in the natural world (1). The timing of migration, and its relative sensitivity to climate, is considered critical for assessing the vulnerability of species and their habitats to future climate change (2). Especially susceptible are facultative migrants whose migratory behavior tracks irregular fluctuations in weather and resources over time and space. Unlike obligate migrants, for which the timing, direction, and distance of seasonal migration are generally consistent from year to year, facultative migrants can breed or winter in the same or widely separated areas during different years, depending on prevailing conditions of food and weather (3, 4).

Particularly interesting is the degree to which unfavorable conditions force migrants out of some areas, whereas favorable conditions elsewhere attract them. Such "push-pull" factors have been described for obligate migrant passerine birds in western North America that are "pushed" away from their breeding grounds by the seasonally dry summers of the western lowlands, whereas wet summers "pull" them south, where the higher productivity associated with the Mexican monsoon can support postbreeding molt. In this case, both molt-migration schedules and pathways for these passerines are modulated by a regional, north-south dipole in seasonal precipitation and productivity (5).

Climatic dipoles can operate at different time scales, and can be defined, via clustering of spatiotemporal data, as climatic anomalies of opposite polarity appearing at two different locations at the same time (6). Notable examples include sea surface temperature (e.g., Tropical Atlantic Sea Surface Temperature Dipole, Indian Ocean Dipole), atmospheric pressure [e.g., Arctic and Antarctic Oscillation, El Niño Southern Oscillation (ENSO), Northern Atlantic Oscillation (NAO)], winter temperature contrasts between eastern and western North America associated with the Arctic Oscillation, and winter precipitation contrasts between the northwestern and southwestern United States in response to ENSO variability. Climatic dipoles involving unfavorable and favorable seasonal conditions drive many obligate (seasonal) migrations, and also could underlie push-pull dynamics in facultative migrations that occur less regularly in space and time.

A particularly dramatic example of facultative migration is avian irruptions, characterized as the broad-scale movement of large numbers of individuals to areas outside their normal range (7–9). In many continents, avian irruptions occur across large geographic areas and display interannual to decadal oscillations (3, 10, 11). Here, we investigate how broad-scale climate variability influences the periodicity, magnitude, and geography of Pine Siskin (*Spinus pinus*) irruptions, an easily identifiable inhabitant of North American boreal forests that has been featured prominently in past analyses of irruptive migrants (12).

Pine Siskins are one of several species of North American seed-eating boreal birds, the most widespread and visible group of irruptive migrants. In some years, these species spend the autumn and winter in the northern coniferous forests, where they breed; in other years, they migrate irregularly to more southerly regions, often hundreds or thousands of kilometers away. These irruptions can occur in a biennial fashion but may also take place in consecutive years or at longer intervals. Because the transition to winter marks a time of resource scarcity for many birds, a prevalent hypothesis for these irruptions is that they are an adaptation that

Significance

This study is the first, to our knowledge, to reveal how climate variability drives irruptions of North American boreal seed-eating birds. Patterns of Pine Siskin irruption and associated climate drivers manifest as two modes (North-South and West-East) in which dipoles of temperature and precipitation anomalies push and pull irruptive movements across the continent at biennial to decadal periodicities. Our study accentuates the value of sustained and synoptic biological observations, contributed by citizen scientists in this case, that match the spatial and temporal scales at which climatic phenomena are observed and understood. Such observations can help probe new questions, such as the role of climatic dipoles in other large-scale ecological processes.

Author contributions: C.S., B.Z., J.L.B., and W.D.K. designed research; C.S. performed research; C.S. analyzed data; and C.S., B.Z., J.L.B., and W.D.K. wrote the paper.

The authors declare no conflict of interest.

This article is a PNAS Direct Submission.

Freely available online through the PNAS open access option.

[1]To whom correspondence should be addressed. Email: court.strong@utah.edu.

This article contains supporting information online at www.pnas.org/lookup/suppl/doi:10.1073/pnas.1418414112/-/DCSupplemental.

allows seed-eating birds in the boreal forest to escape widespread food shortages associated with the "boom-and-bust" economy of masting (11), the spatially synchronized and highly variable production of copious seed across populations of conifers and other perennial plants (13, 14). Masting incurs expensive reproductive costs over one or more years, and resources depleted by synchronized reproduction in one year can lead to poor seed crop production in the next year (14–16). Limited historical data for boreal conifer masting and avian irruptions exhibit inverse correlations, with boreal birds greatly expanding their winter ranges, north to south or west to east, a year after the masting event (10, 11). How large-scale patterns in climate, wintering habitat conditions, and seed production interact to push and/or pull boreal bird irruptions across the continent remains largely unknown.

Monitoring of conifer seed production is patchy throughout North American boreal forests, but available data suggest that the timing of resource accumulation and seed production can be driven by climate variability across broad scales (17). Reproductive cycles typically span 2 to 3 y in boreal conifers, and climatic conditions in the years preceding a masting event have been shown to be critical in pines (*Pinus* spp.) (18, 19), balsam fir (*Abies balsamea*) (20), white spruce (*Picea glauca*) (21, 22), and black spruce (*Picea mariana*) (23). Many of these studies suggest that masting is favored by a warm, dry spring and summer in the year of cone initiation and a warm summer in the subsequent year. Even more complicated climate pathways have been suggested, including instances in which conditions during the previous two summers before masting, and the temperature difference between the two previous summers in some cases, best predict seed crops (16). These response functions may explain why both masting and tree growth can be synchronized within and across different conifer species over scales ranging from 500–1,000 km (24).

Climate-mediated pulses of seed production have the potential to impart periodicity to avian irruptions through demographic cascades. Prior studies support the idea that pulses in seed production trigger increases in bird populations that, through local food shortage and other density-dependent processes, can lead to irruptive migration events in the following year. For example, studies on boreal seed-dependent birds have found juvenile-to-adult ratios varying from 3.54 in years of high seed production to 0.33 in years of low seed production (25). Common Redpolls (*Acanthis flammea*) and Pine Siskins can breed twice as long in mast years than in other years (two to three broods instead of one to two broods) (26), and total reproductive failure has been noted during years following masting events (8). Irruptions of birds take many forms, but because seed production may be greatly diminished after a masting event, it is generally assumed that individuals benefiting from masting in one year may be forced to move great distances in search of food the following winter.

Despite having been a subject of ecological interest for many decades (27), the environmental and climatic forces that drive avian irruptions remain a mystery for at least two reasons. First, irruptive migrants are difficult to track, and documenting their shifting distributions requires data collected from multiple sites separated by hundreds or thousands of kilometers. Second, the potential drivers of irruptions occur over broad spatiotemporal scales that are difficult to evaluate locally or over the short term. In recent years, however, climate data reanalysis products and long-term and continent-wide observations of wintering birds by citizen scientists offer opportunities to disentangle the effects of regional climate variability on irruptions.

One possible mechanism for climatic forcing involves direct and immediate forcing of irruptive patterns by harsh winters. This hypothesis follows many studies that have tested the influence of the NAO and other climate indices on changes in seasonal migration phenology (28). Another possible role for climate involves imparting periodicity of avian irruption patterns through lagged influences on cone development and masting in the boreal forest. In this case, climate would indirectly modulate irruptions via sequential, multiyear climatic conditions favorable for widespread masting. The role of climate variability and the degree to which boreal seed-eating birds are pushed away by seed scarcity in their wintering ranges, while simultaneously being pulled elsewhere by the presence of large cone crops, has not been previously established.

To investigate climate influences on irruptions, we analyzed gridded climate datasets alongside long-term bird observations from Project FeederWatch, an international citizen science program that monitors the occurrence and abundance of wintering birds at supplemental feeding stations throughout North America. The FeederWatch database is ideal for associating bird occurrence and abundance observations with gridded climate data because of its continuous winter sampling protocol (early November through early April), annual time series (1989–2012), and large sample size (>10,000 participants per year).

Pine Siskins forage primarily on plant seeds (>70% of their diet) (29) and demonstrate known irruptive migration movements at a continental scale and of varying periodicity. Fig. 1 shows the range of Pine Siskins in North America (12) and the FeederWatch observation domain. During nonirruptive years, the range in eastern North America is largely restricted to northern coniferous forests of Canada, a region dominated by firs (*Abies* spp.), spruces (*Picea* spp.), larches (*Larix* spp.), and pines (*Pinus* spp.). During irruptive years, Pine Siskins have been observed in high-elevation forests of the Appalachian and Adirondack Mountains, and sparse banding recoveries in years following these irruptions demonstrate a south-southwest/north-northeast spring migration trajectory possibly reflecting the orientation of eastern mountains and the Atlantic coastline (12). In western North America, Pine Siskins are year-round residents and generally

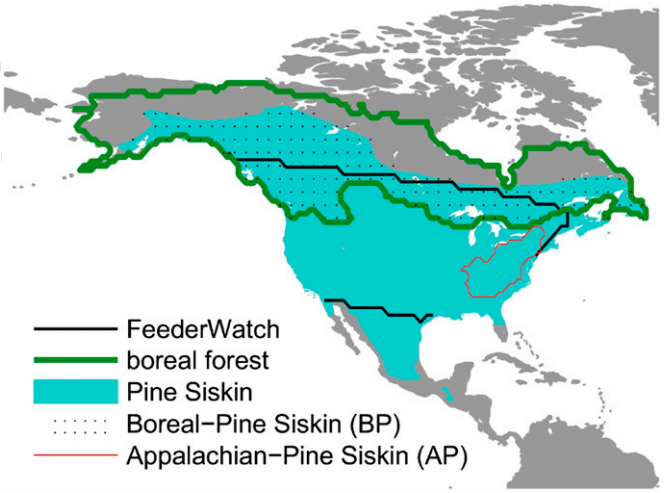

Fig. 1. Pine Siskin range and key subregions. Blue shading indicates the range of the Pine Siskin over North America (32). The black contours show the northern and southern edges of the FeederWatch observation domain. The green contour indicates the boreal forest (59), and the intersection of the boreal forest and Pine Siskin range (stippling) is referred to as the BP region. The BP region is expansive; located mostly in Canada; and dominated by firs (*Abies* spp.), spruces (*Picea* spp.), larches (*Larix* spp.), and pines (*Pinus* spp.), providing favorable conditions for year-round residency of Pine Siskins (32). The area within the red contour is referred to as the AP region, and is composed of six physiographic provinces (60) within the range of the Pine Siskin: piedmont, Blue Ridge, valley and ridge, Appalachian plateaus, Adirondack, and interior low plateaus. The AP region features high-elevation conifer forests and mixed deciduous lowland forests typical of the eastern United States, and coniferous seeds provide a resource pool for Pine Siskins during irruptions over the eastern United States.

inhabit montane coniferous or mixed forests. Although these populations show less broad-scale variability in irruptive movements relative to their eastern counterparts, they exhibit altitudinal shifts in spring and autumn (12, 30).

Results

Patterns of Pine Siskin Count Variability. FeederWatch Pine Siskin count maps for each year of the available record (1989–2012) revealed dramatic interannual variation. For example, the winter ending in 1990 featured a spectacular irruption or "superflight" south of the boreal forest (Fig. 2*A*), and, by contrast, the winter ending in 2004 featured near absence of Pine Siskins over the contiguous United States (Fig. 2*B*). The winter ending in 2009 featured another irruption with high counts south of the boreal forest (Fig. 2*C*), followed by greatly reduced counts in the subsequent winter (Fig. 2*D*). West-east shifts in the spatial distribution of Pine Siskins across the boreal forest were also evident. For example, the winter ending in 1995 featured relatively high counts over the eastern boreal forest (Fig. 2*E*), whereas the winter ending in 2002 featured relatively high counts over the western boreal forest (Fig. 2*F*). The aforementioned patterns are reflected in the first two modes of variability presented in the next section.

Objective Identification of Irruption Modes. From FeederWatch counts (e.g., Fig. 2), we established a Pine Siskin count time series (1989–2012) for each of 1,003 grid point locations over the FeederWatch domain and then analyzed the 1,003 time series simultaneously using empirical orthogonal function (EOF) analysis (31), also known as principal components analysis. For each principal mode of count variability within the FeederWatch domain, this analysis yielded a time series indicating the sign and magnitude of the mode (index time series; e.g., Fig. 3*A*). The mode's spatial pattern was shown by mapping the correlation between the index time series and the Pine Siskin count time series at each grid location (e.g., Fig. 3*B*). More formally, the spatial pattern of each principal mode was defined by an eigenvector of the spatial correlation matrix. Maps of these eigenvector components are shown in Fig. S1, and additional mathematical details of the EOF analysis are provided in *Methods*.

The principal modes of variability were ordered so that the first mode accounted for the largest fraction of the total variance, the second mode accounted for the second largest fraction, and so on. The first mode, hereafter referred to as the North-South Irruption Mode, accounted for 42% of the total variance. The North-South Irruption Mode index (Fig. 3*A*) exhibited multidecadal periodicity with large positive values in 1990 and 2009, two prominent irruption years (Fig. 2 *A* and *C*). Correlation between the North-South Irruption Mode index and the Pine Siskin count time series at each grid location featured a negative correlation (smaller counts when the index is positive; blue shading in Fig. 3*B*) over a relatively small region in the western boreal forest and a positive correlation (larger counts when the index is positive; red shading in Fig. 3*B*) over much of the contiguous United States.

The second mode of Pine Siskin count variability, hereafter referred to as the West-East Irruption Mode, accounted for 13% of the total variance. The West-East Irruption Mode index (Fig. 4*A*) exhibited prominent biennial fluctuations before 2000, with increased temporal irregularity thereafter. Correlation between the West-East Irruption Mode index and the Pine Siskin count time series at each grid location highlighted regions in the western and eastern boreal forest where the correlations were strongly negative (blue shading in Fig. 4*B*) or strongly positive (red shading in Fig. 4*B*), respectively.

The variability patterns for the first and second modes (Figs. 3*B* and 4*B*) suggest that the West-East Irruption Mode dominated the boreal forest region and the North-South Irruption Mode dominated the region south of the boreal forest. To confirm, we also analyzed FeederWatch domain variability within the boreal forest alone and then in the area south of the boreal forest. For the portion of the FeederWatch domain south of the boreal forest, the leading mode of variability (Fig. S1*G*) was nearly identical to the North-South Irruption Mode (temporal correlation of index time series: $r = 0.99$; Fig. S1*D*) and accounted for 56% of the variance. Within the boreal forest portion of the FeederWatch domain alone, the leading mode of variability (Fig. S1*H*) was very similar to the West-East Irruption Mode (temporal correlation of the index time series: $r = 0.92$; Fig. S1*E*) and accounted for 39% of the variance.

Finally, the third mode of Pine Siskin count variability over the entire FeederWatch domain (Fig. S1*C*) accounted for 11% of the total variance. This mode achieved an exceptionally strong negative value in 1993 with weaker fluctuations in other years of the record (Fig. S1*F*). In contrast to the first and second modes, we were not able to establish that the third mode of variability represented the leading mode within any objectively defined domain, and thus do not consider it further.

Climate Drivers of the North-South Irruption Mode. We developed maps showing the correlation between the North-South Irruption Mode index (Fig. 3*A*) and near-surface air temperature and precipitation time series at each grid point location over North America. Correlation maps were developed separately for four

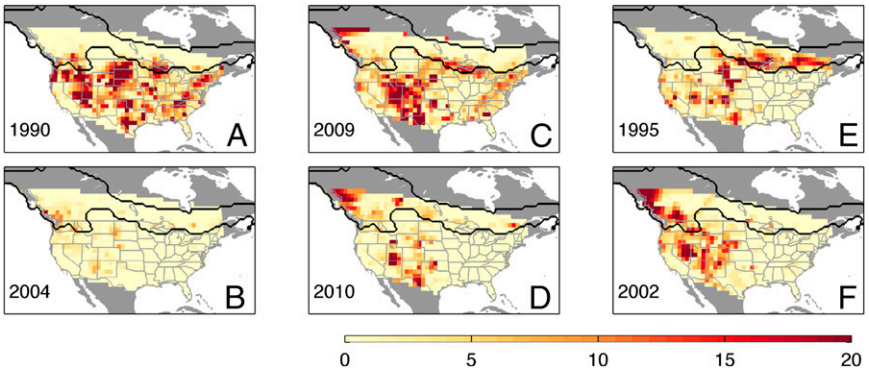

Fig. 2. Pine Siskin count variability. (*A–F*) Pine Siskin counts for years indicated at the lower left of each panel are shown. The shaded values (scaled 0–20) are the inverse distance-weighted average of the once-per-week tallies of Pine Siskins reported by Project FeederWatch participants located within 100 km of the grid point (*Methods, FeederWatch Counts*). For each weekly tally, participants observed feeders for two consecutive days and reported the largest number of Pine Siskins observed at any one time. Gray shading indicates land areas not monitored by Project FeederWatch. The BP region is outlined in black.

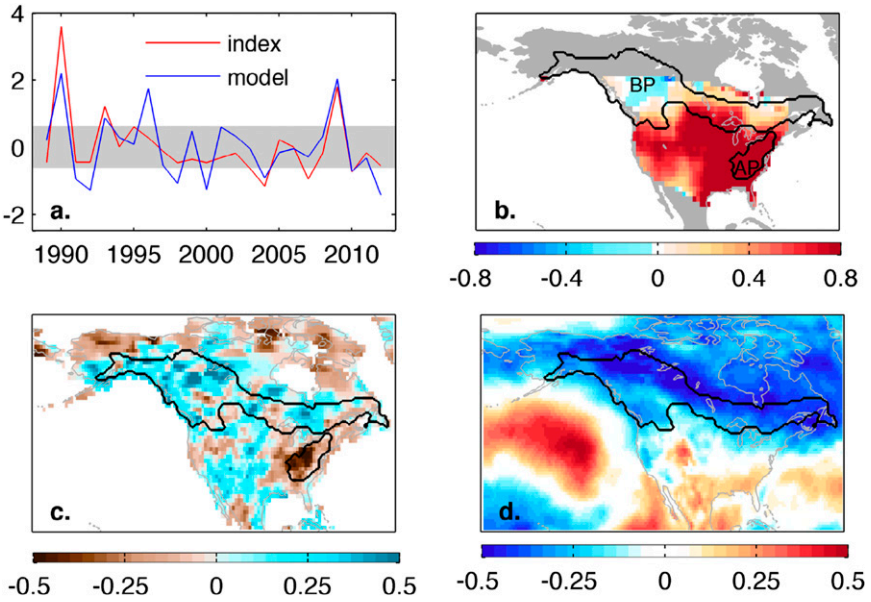

Fig. 3. North-South Irruption Mode and associated climate drivers. (*A*) North-South Irruption Mode index (red curve) is the time series that accounts for the largest fraction of variability (42%) in Pine Siskin counts over the period of record (1989–2012). The blue curve is a statistical model of the North-South Irruption Mode index constructed from climate indices as detailed in the main text (Eq. **1**). Index values outside the gray shading are referred to as "exceptional" (absolute value greater than 0.6), and examples of years with exceptional positive and negative index values are shown in Fig. 2 *A* and *B*, respectively. (*B*) Spatial pattern of the North-South Irruption Mode is shown by the correlation (*r*) between the North-South Irruption Mode index and the Pine Siskin count time series at each location (shading). The BP region and AP region are outlined in black. (*C*) Correlation of North-South Irruption Mode index with spring (March through May) precipitation from the preceding year (y_{-1}). (*D*) Correlation of North-South Irruption Mode index with winter (December through February) air temperature from the contemporaneous year (y_0).

seasons and lags of 0, 1, and 2 y (e.g., Fig. 3 *C* and *D*). From comparison of the correlation maps and the spatial pattern of the North-South Irruption Mode (Fig. 3*B*), we identified two physiographic regions where climate variability was a physically plausible driver of North-South irruption: the Boreal-Pine Siskin (BP) region and the Appalachian-Pine Siskin (AP) region (these

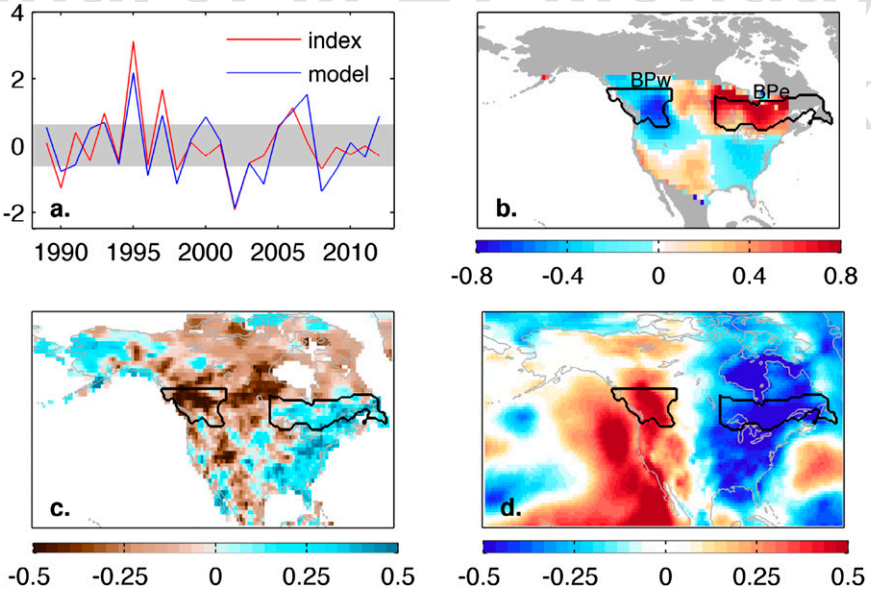

Fig. 4. West-East Irruption Mode and associated climate drivers. (*A*) West-East Irruption Mode index (red curve) is the time series that accounts for the second largest fraction of variability (13%) in Pine Siskin counts over the period of record (1989–2012). The blue curve is a statistical model of the West-East Irruption Mode index constructed from climate indices as detailed in the main text (Eq. **2**). Index values outside the gray shading are referred to as "exceptional" (absolute value greater than 0.6), and examples of years with exceptional positive and negative index values are shown in Fig. 2 *E* and *F*, respectively. (*B*) Spatial pattern of the West-East Irruption Mode is shown by the correlation between the West-East Irruption Mode index and the Pine Siskin count time series at each location (shading). Subsections of the BP region are indicated by black contours: a BPw portion bounded by 56° N and 110° W and a BPe portion bounded by 95° W. (*C*) Correlation of West-East Irruption Mode index with summer (June through August) precipitation from y_{-2}. (*D*) Correlation of West-East Irruption Mode index with summer air temperature from y_{-2}.

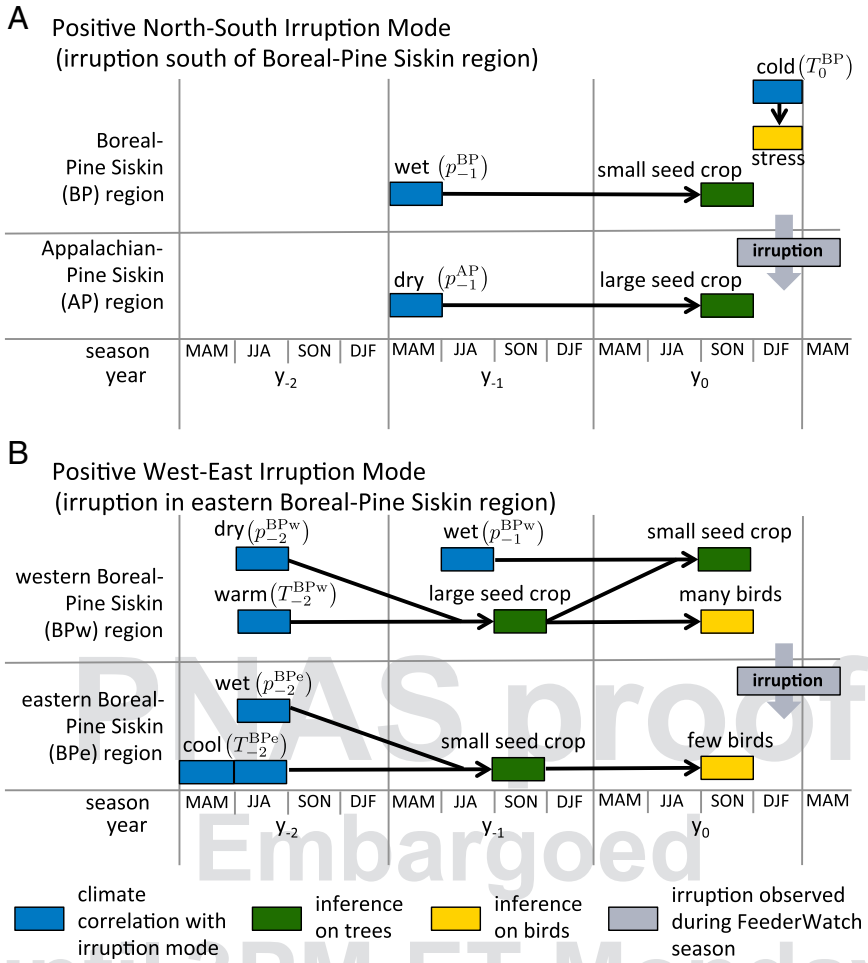

Fig. 5. Irruption mechanisms. (*A*) Timing of events associated with the positive phase of the North-South Irruption mode. The notation used for the climate drivers (blue boxes) follows the conventions established in Table 1. (*B*) Timing of events associated with the positive phase of the West-East Irruption Mode. The notation used for the climate drivers (blue boxes) follows the conventions established in Table 2. At the lower edge of each panel, seasons are abbreviated as follows: spring is March through May (MAM), summer is June through August (JJA), autumn is September through November (SON), and winter is December through February (DJF). Gray arrows indicate the direction of migration associated with the irruption.

regions are labeled in Fig. 3*B*, and their physical and ecological characteristics are detailed in the legend for Fig. 1). The western United States, despite having an expansive coniferous forest where Pine Siskins are year-round residents (32), showed relatively weak correlations between climate variability and the North-South Irruption index (e.g., Fig. 3 *C* and *D*).

Correlations between the North-South Irruption Mode index and average temperature over the BP region and AP region were calculated for four seasons and three temporal lags; seasons and lags are shown schematically in Fig. 5, where the year contemporaneous with FeederWatch is denoted y_0, 1 y prior is denoted y_{-1}, and 2 y prior is denoted y_{-2}. Similar calculations were performed for precipitation. Three of the calculated correlations were significant at the 95% confidence level (Table 1). Beginning with the first two rows of Table 1, the North-South Irruption Mode index was positively correlated with spring y_{-1} precipitation over the BP region and negatively correlated with spring y_{-1} precipitation over the AP region (Fig. 3*C*). The oppositely signed precipitation correlations suggest a dipole pattern, where anomalously wet conditions over the BP region occurred together with anomalously dry conditions over the AP region. The tendency for these precipitation anomalies to occur together is confirmed by the negative correlation between spring y_{-1} precipitation over the BP and AP regions (correlation coefficient: $r = -0.44$, significant at $P < 0.05$); this correlation increased to $r = -0.90$ ($P < 0.05$) when the analysis was restricted to years with exceptional values of the North-South Irruption Mode index (years outside the gray shading in Fig. 3*A*). The North-South Irruption Mode index was negatively correlated with contemporaneous winter air temperature over the BP region (row c in Table 1 and blue shading in Fig. 3*D*), suggesting a direct influence of climate on the North-South Irruption Mode. This strong direct linkage of winter air temperature on Pine Siskin

Table 1. North-South Irruption Mode climate correlations

Row	Variable	Region	Year	Months	Notation	*r*
a	Precipitation	BP	y_{-1}	March–May	Spring p_{-1}^{BP}	0.64
b	Precipitation	AP	y_{-1}	March–May	Spring p_{-1}^{AP}	−0.51
c	Temperature	BP	y_0	December–February	Winter T_0^{BP}	−0.40

Correlation (*r*) of North-South Irruption Mode index with precipitation and air temperature indices. In the notation column, the superscript indicates the region over which the climate data were spatially averaged (the BP region or the AP region; Fig. 1) and the subscript indicates lag (e.g., subscript −1 indicates that climate data were taken from y_{-1}, as illustrated schematically in Fig. 5). All correlation coefficients are significant at the 95% confidence level.

irruption patterns is surprising, given the species' cold hardiness (33).

Seed crop data could, in principle, confirm the above-identified linkages between spring precipitation variability and migration. In lieu of such data, which are unfortunately too sparse to match the spatial and temporal scales of this study, we made inferences about conifer seed crop size that are consistent with tree reproductive theory and output from models developed to make weather-based conifer seed crop predictions (17–22, 34–37). Specifically, an anomalously warm or dry spring or summer favors budding and pollination, yielding a large seed crop (masting) during the next year's autumn, whereas an anomalously cool or wet spring or summer yields a small seed crop during autumn of the following year. In addition, mast years tend to promote a diminished seed crop during the following year because trees presumably must replenish their reserves after a mast year (38), although masting generally does not follow a strictly biennial pattern and can occur over consecutive years. Combining the seed inferences and climate-irruption correlations, Fig. 5*A* shows a schematic summary of the proximate mechanisms for the extreme positive phase of the North-South Irruption Mode (Pine Siskins irrupting south over the eastern United States). The sequence of events starts in y_{-1}, with a wet spring in the BP region and a dry spring in AP region (blue boxes in y_{-1} in Fig. 5*A*). The positive phase of the North-South Irruption Mode is then triggered in y_0 by a seed-poor winter over the BP region in conjunction with a seed-rich winter over the AP region (green boxes in y_0 in Fig. 5*A*), together with an especially cold winter over the BP region (blue box in y_0 in Fig. 5*A*).

Finally, we evaluated the extent to which the three climate variables in Table 1 collectively explained variations in the North-South Irruption Mode by using the variables to construct a statistical model of the North-South Irruption Mode index. The model was constructed using forward stepwise regression (39). Proceeding in a stepwise fashion, a predictor was included in the model only if its addition was significant at $P \leq 0.05$ based on an *F* test. Using the notation from Table 1 and standardizing the predictors to facilitate interpretation of the regression coefficients, the resultant statistical model (*N*) of the North-South Irruption Mode index

$$N = 0.57 \cdot \text{spring}\ p_{-1}^{BP} - 0.41 \cdot \text{winter}\ T_0^{BP} \quad [1]$$

accounted for 58% of the variance in the North-South Irruption Mode index ($r = 0.76$; blue curve in Fig. 3*A*). The stepwise procedure parsimoniously excluded the precipitation index from the AP region (row b in Table 1) because of its previously noted correlation ($r = -0.44$, significance at $P < 0.05$) with the precipitation index from the BP region (row a in Table 1).

Climate Drivers of the West-East Irruption Mode. For the West-East Irruption Mode, we performed a climate correlation mapping analysis analogous to the analysis described above for the North-South Irruption Mode. From comparison of the correlation maps (e.g., Fig. 4 *C* and *D*) and the spatial pattern of the West-East Irruption Mode (Fig. 4*B*), we identified two physiographic regions where climate variability was a plausible driver of irruption: the western Boreal-Pine Siskin (BPw) region (Fig. 4*B*) and the eastern Boreal-Pine Siskin (BPe) region (Fig. 4*B*). We then analyzed the West-East Irruption Mode index's correlation with temperature over the BPe region and the BPw region for four seasons and three temporal lags (y_0, y_{-1}, and y_{-2}). Similar calculations were completed for precipitation. Six of these calculated correlations were significant at the 95% confidence level (listed in Table 2).

The correlation results captured a striking continental-scale west-east dipole of warm-season precipitation and temperature anomalies (Fig. 4 *C* and *D*). Specifically, positive values of the West-East Irruption Mode index tended to follow (at a 2-y lag) anomalously warm and dry summer conditions over western North America (brown shading in Fig. 4*C* and red shading in Fig. 4*D*) paired with anomalously cool and wet summer conditions over eastern North America (blue shading in Fig. 4 *C* and *D*). Oppositely signed spring climate anomalies were not reliably present over North America, as reflected in the weak overall correlation between spring y_{-2} precipitation in the BPw and BPe regions ($r = -0.34$, $P = 0.14$), but restricting the analysis to years with exceptional values of the West-East Irruption Mode index (years outside gray shading in Fig. 4*A*) strengthened the BPw region and BPe region springtime precipitation correlation to $r = -0.65$ ($P = 0.08$).

Table 2. West-East Irruption Mode climate correlations

Row	Variable	Region	Year	Months	Notation	*r*
a	Precipitation	BPw	y_{-1}	June–August	Summer p_{-1}^{BPw}	0.45
b	Precipitation	BPw	y_{-2}	June–August	Summer p_{-2}^{BPw}	−0.55
c	Temperature	BPw	y_{-2}	June–August	Summer T_{-2}^{BPw}	0.50
d	Temperature	BPe	y_{-2}	March–May	Spring T_{-2}^{BPe}	−0.49
e	Precipitation	BPe	y_{-2}	June–August	Summer p_{-2}^{BPe}	0.43
f	Temperature	BPe	y_{-2}	June–August	Summer T_{-2}^{BPe}	−0.55

Correlation (*r*) of West-East Irruption Mode index with precipitation and air temperature indices. In the notation column, the superscript indicates the region over which the climate data were spatially averaged (the BPw region or the BPe region; Fig. 4*B*) and the subscript indicates lag (e.g., subscript −1 indicates that climate data were taken from y_{-1}, as illustrated schematically in Fig. 5). All correlation coefficients are significant at the 95% confidence level.

For each of the six climate indices (Table 2), plausible roles in driving the positive phase of the West-East Irruption Mode (eastward migration of Pine Siskins) are illustrated schematically in Fig. 5*B*. The y_{-2} temperature and precipitation drivers in the BPw region (two blue boxes in y_{-2}, upper row of Fig. 5*B*) follow the classical irruption sequence: Warm and dry conditions during summer of y_{-2} lead to a resource pulse of a large seed crop in y_{-1}, supporting high recruitment and a large Pine Siskin population in the BPw region by autumn of y_0. Further stressing y_0 conditions in the west, the seed crop in autumn of y_0 will tend to be small because trees must replenish their reserves after the strong y_{-1} crop (38), and wet conditions during summer y_{-1} further depress y_0 crop size. Meanwhile, the three temperature and precipitation drivers in the BPe region (three blue boxes in y_{-2}, lower row of Fig. 5*B*) build a sequence nearly opposite to the sequence of the BPw region: wet conditions during summer of y_{-2} and cool conditions during spring and summer of y_{-2} weaken the y_{-1} seed crop, resulting in weak recruitment and a small Pine Siskin population leading into the y_0 FeederWatch season. Summarizing Fig. 5*B*, the extreme positive phase of the West-East Irruption Mode (eastward migration of Pine Siskins) appeared to be triggered by the classical irruption sequence in the BPw region (large population with limited seed resources) in conjunction with a diminished population in the BPe region. This dynamic potentially supports a migration pattern where siskins move back and forth across the coniferous forests from Alaska to Newfoundland searching for cone crops, a "pendulum" flight pattern that has previously been noted for Crossbill (*Loxia curvirostra*) invasions in Great Britain (40).

Finally, we evaluated the extent to which the six climate variables in Table 2 collectively explain variations in the West-East Irruption Mode by using the variables to construct a statistical model of the West-East Irruption Mode index. The model was constructed using forward stepwise regression (39). Proceeding in a stepwise fashion, a predictor was included in the model only if its addition was significant at $P \leq 0.05$ based on an *F* test. Using the notation in Table 2 and standardizing the predictors to facilitate

interpretation of the regression coefficients, the resultant statistical model (W) of the West-East Irruption Mode index

$$W = 0.42 \cdot \text{summer } T_{-2}^{BPw} - 0.34 \cdot \text{spring } T_{-2}^{BPe} - 0.37 \cdot \text{summer } T_{-2}^{BPe} \quad [2]$$

accounted for 58% of the variance in the West-East Irruption Mode index ($r = 0.76$; blue curve in Fig. 4*A*). The stepwise procedure parsimoniously excluded the precipitation indices, partially because temperature and precipitation were strongly negatively correlated at the same location and time (e.g., $r = -0.59$ for summer p_{-2}^{BPw} and summer T_{-2}^{BPw}). In contrast, the stepwise procedure included all of the temperature indices in the model because they were not always synchronized between regions and seasons, but when they did synchronize, they tended to produce extreme positive or negative values of the West-East Irruption Mode index.

Discussion

We decomposed patterns of Pine Siskin irruptions into two continental modes: a North-South Irruption Mode with prominent irruptions in 1990 and 2009 and a West-East Irruption Mode with biennial fluctuations before 1998 followed by more erratic temporal variability. In contrast to prior studies (10), we uncovered statistically significant and physically plausible climate drivers for each irruption mode. Most of the climate drivers were precipitation or temperature effects preceding the winter FeederWatch observation season by 1 or 2 y, and the success of the statistical models presented here indicates that irruptions may be predictable. Any such increase in predictability would potentially provide an opportunity to understand irruptions better through the marking and subsequent following of birds during irruption events. It might further facilitate the ability to detect their ecological consequences, which, like other pulsed phenomena, are potentially significant (41, 42).

For both irruption modes, the predominant climate forcing had a dipole spatial structure, meaning that the climate forcing tended to produce an unfavorable seed crop over one region (cool-wet forcing) and a favorable seed crop over another (warm-dry forcing). Although hypotheses for avian irruptions have generally focused on a sequence of conditions leading to the demographic consequences of food shortages in the region from which birds migrate, our results are more consistent with a push-pull paradigm in which antiphased climate anomalies (dipoles) modulate broad-scale irruptions by creating unfavorable conditions in one region and more favorable conditions in another. The pull of irruptive migrants and settlement in a region could result from social cues in decision making, such as conspecific attraction (43), for choosing suitable wintering habitat. Based on our findings, however, this dynamic is probably stronger for the North-South Irruption Mode (large y_0 seed crop in the AP region; Fig. 5*A*) than it is for the West-East Irruption Mode (fewer birds in the BPe region; Fig. 5*B*). For the western United States, there was some tendency for above-average Pine Siskin counts during North-South irruption (red shading in Fig. 3*B*), yet climate in this region did not strongly correlate with the North-South Irruption Mode index. This lack of a straightforward climate connection suggests that a component of western US irruption is more push than pull (i.e., some Pine Siskins migrating south from unfavorable conditions in the boreal forest arrive in the western United States even though conditions in this region are not especially favorable). However, conclusions about the mountainous western United States are complicated by relatively low observation densities in the FeederWatch data, strong elevation gradients, heterogeneity in conifer masting (44), and underlying fluctuations in local resident bird populations.

The climate drivers of Pine Siskin irruptions are regional manifestations of larger scale climate patterns. The precipitation dipole underlying the North-South Irruption Mode is similar to a dipole pattern other studies have identified as the leading mode of annual mean precipitation variability over eastern North America (45), and the winter air temperature driver of the North-South Irruption Mode is correlated with the North Pacific Index (46) ($r = -0.50$, $P < 0.05$). The North Pacific Index is linked to hemispheric modes of decadal circulation variability (47) and tracks sea level pressure variations that strongly influence temperature extremes (48). The precipitation and temperature dipoles associated with the West-East Irruption Mode are, in part, driven by a pan-Pacific atmospheric wave pattern emanating from Asian monsoonal convection (49), and similar warm-season climate dipoles have been more generally linked to Rossby wave-like structures guided by the mean jet streams over North America (50) and Asia (51).

Nearly half of all North American birds breed in the boreal forest (52), and as such, the periodicity of avian irruptions, and their connection to climate, likely represents a critical bellwether of how climate variability influences North American biota. Climate change may alter the strength, periodicity, synchrony, or orientation of the irruptive patterns identified here because future changes in spring and summer precipitation are projected to exhibit varying dipole patterns over North America (53). The implication for species that display strong variability in population dynamics (irruptions and cycling) may be a future characterized by uncertain changes in climate and resources.

We were able to uncover linkages between climate and continent-wide avian irruptions by leveraging rich data from an international citizen science program and making mechanistically consistent inferences on regional seed crop variability. Deeper understanding of these correlations will be possible as more comprehensive spatiotemporal data, particularly on seed production, become available. Finally, precipitation and temperature dipoles are common and well-known features in the climate system, and their influence could extend well beyond boreal bird irruptions to explain a broad suite of important biogeographic phenomena.

Methods

FeederWatch Counts. Counts for each FeederWatch season (beginning the second Saturday in November and running for 21 wk) were arranged onto a spatial grid by averaging reported tallies within 100 km of each grid point using inverse square-root distance weighting (54). This weighting follows the convention used by the Cornell Lab of Ornithology for the online FeederWatch Map Room, and grid spacing was set to $\sqrt{2 \cdot 100^2}$ km to ensure all data records were used at least once. This procedure provides 1,003 grid points over the FeederWatch domain. For each weekly tally, participants observed their feeders for two consecutive days and reported the largest number of Pine Siskins observed at any one time. Each participant could provide up to 21 tallies per year (one for each week of the FeederWatch season). To minimize the impacts of participants joining or leaving during a 21-wk season, the gridding procedure was applied separately to three 7-wk segments of each season, and the three 7-wk results were then averaged with equal weight to produce a count map for each of the 24 available years (1989–2012). To deemphasize small-scale heterogeneity inherent in the FeederWatch data, each count map was smoothed using a moving average filter assigning equal weights over a square with a 100-km edge.

FeederWatch Leading Modes. The modes of Pine Siskin count variability were objectively determined by performing EOF analysis (55). In this application, the variables were the standardized time series of Pine Siskin count at each of $n = 1{,}003$ grid points, and each time series was of length $m = 24$ y. These variables were assembled into a $m \times n$ matrix, and each EOF was an eigenvector of the associated $n \times n$ spatial covariance matrix. In this way, the EOFs were spatial basis functions (vectors of length n). The associated expansion functions (index time series or "principal components") were projections of the standardized data onto the spatial basis functions. Rather than mapping the EOF basis function (an arbitrarily scaled and dimensionless eigenvector), it is customary (56) to map the regression coefficients obtained by regressing the centered (scaled to zero-mean) data onto the index time series or, as shown in Figs. 3*B* and 4*B*, the correlation between the index time series and

the raw time series at each grid point. The EOF basis functions themselves are shown in Fig. S1 *A–C*.

Climate Data. We analyzed climate data for the period 1985–2012, which corresponds to the FeederWatch data period plus the preceding 4 y for lag analysis. For precipitation (*p*), we used the Global Precipitation Climatology Centre (GPCC) monthly dataset (57) on a 1° grid. For 1901–2010, GPCC version 6 is based on quality-controlled data from 67,200 stations worldwide with record durations of at least 10 y. For 2011 to the present, GPCC is a "monitoring product" based on quality-controlled data from 7,000 stations. Sea level pressure and air temperature at 2 m above the ground were based on daily, full-resolution (nominally 80-km horizontal grid) data from European Centre for Medium-Range Weather Forecasts Interim Reanalysis (ERA-Interim) (58). We used area weighting and temporal averaging to construct precipitation and air temperature indices for specific seasons and objectively defined regions (e.g., BP region in Fig. 1).

ACKNOWLEDGMENTS. We are indebted to thousands of volunteers that participate in Project FeederWatch. We thank David N. Bonter and the Cornell Lab of Ornithology for access to FeederWatch data and Karine Princé for data management. We thank the editor and two anonymous reviewers for comments that helped to improve the manuscript. The interdisciplinary collaboration that led to this paper was facilitated by a Research Coordination Network workshop on continental-scale phenological modeling in Milwaukee funded by National Science Foundation Grant IOS-0639794 and supported by the USA National Phenology Network. Additional support was received from National Science Foundation Grant DEB-1256394 (to W.D.K.).

1. Berthold P, Gwinner E, Sonnenschein E (2003) *Avian Migration* (Springer, New York).
2. Cox GW (2010) *Bird Migration and Global Change* (Island Press, Washington, DC).
3. Newton I (2008) *Bird Migration* (Academic, London).
4. Newton I (2012) Obligate and facultative migration in birds: ecological aspects. *J Ornithol* 153(1):171–180.
5. Rowher S, Butler LK, Froehlich SR (2005) Ecology and demography of east-west differences in molt scheduling of neotropical migrant passerines. *Birds of Two Worlds: The Ecology and Evolution of Migration*, eds Greenberg R, Marra PM (Johns Hopkins Univ Press, Baltimore, MD), pp 87–106.
6. Nigam S, Baxter S (2015) Teleconnections. *Encyclopedia of Atmospheric Sciences*, eds North G, Zhang F, Pyle J (Academic, London), 2nd Ed, pp 90–109.
7. Lack DL (1954) *The Natural Regulation of Animal Numbers* (Clarendon, Oxford).
8. Newton I (1972) *Finches* (Collins, London).
9. Newton I (1970) Irruptions of crossbills in Europe. *Populations in Relation to Their Food Resources*, ed Watson A (Blackwell, Oxford), pp 337–357.
10. Koenig WD, Knops JMH (2001) Seed-crop size and eruptions of North American boreal seed-eating birds. *J Anim Ecol* 70(4):609–620.
11. Larson DL, Bock CE (1986) Eruptions of some North American boreal seed-eating birds, 1901-1980. *Ibis* 128(1):137–140.
12. Dawson WR (1997) Pine Siskin (*Spinus pinus*). The Birds of North America Online, ed Poole A (Cornell Laboratory of Ornithology, Ithaca, NY). Available at bna.birds.cornell.edu/bna/species/280. Accessed February 5, 2015.
13. Koenig WD, Knops JMH (2005) The mystery of masting in trees. *Am Sci* 93(4):340–347.
14. Kelly D, Sork VL (2002) Mast seeding in perennial plants: Why, how, where? *Annu Rev Ecol Syst* 33:427–447.
15. Koenig WD, Knops JMH (2000) Patterns of annual seed production by northern hemisphere trees: a global perspective. *Am Nat* 155(1):59–69.
16. Kelly D, et al. (2013) Of mast and mean: Differential-temperature cue makes mast seeding insensitive to climate change. *Ecol Lett* 16(1):90–98.
17. Owens JN, Blake MD (1985) *Forest Tree Seed Production: A Review of the Literature and Recommendations for Future Research. Information Report PI-X-53* (Canadian Forest Service, Petawawa National Forestry Institute, Chalk River, Ontario, Canada).
18. Houle G, Filion L (1993) Interannual variations in the seed production of *Pinus-banksiana* at the limit of the species distribution in northern Quebec, Canada. *Am J Bot* 80(11):1242–1250.
19. Mooney KA, Linhart YB, Snyder MA (2011) Masting in ponderosa pine: Comparisons of pollen and seed over space and time. *Oecologia* 165(3):651–661.
20. Messaoud Y, Bergeron Y, Asselin H (2007) Reproductive potential of balsam fir (*Abies balsamea*), white spruce (*Picea glauca*), and black spruce (*P. mariana*) at the ecotone between mixedwood and coniferous forests in the boreal zone of western Quebec. *Am J Bot* 94(5):746–754.
21. Juday GP, Barber V, Rupp S, Zasada JC, Wilmking M (2003) A 200-year perspective of climate variability and the response of white spruce in interior Alaska. *Climate Variability and Ecosystem Response at Long-Term Ecological Research Sites*, eds Greenland D, Goodin DG, Smith RC (Oxford Univ Press, Oxford), pp 226–250.
22. Krebs CJ, LaMontagne JM, Kenney AJ, Boutin S (2012) Climatic determinants of white spruce cone crops in the boreal forest of southwestern Yukon. *Botany* 90(2):113–119.
23. Sirois L (2000) Spatiotemporal variation in black spruce cone and seed crops along a boreal forest-tree line transect. *Can J For Res* 30(6):900–909.
24. Koenig WD, Knops JMH (1998) Scale of mast-seeding and tree-ring growth. *Nature* 396(6708):225–226.
25. Lindstrom A, Enemar A, Andersson G, von Proschwitz T, Nyholm NEI (2005) Density-dependent reproductive output in relation to a drastically varying food supply: Getting the density measure right. *Oikos* 110(1):155–163.
26. Shaw G (1990) Timing and fidelity of breeding for siskins *Carduelis spinus* in Scottish conifer plantations. *Bird Study* 37(1):30–35.
27. Reinikainen A (1937) The irregular migrations of the Crossbill, *Loxia c. curvirostra*, and their relation to the cone-crop of the conifers. *Ornis Fennica* 14:55–64.
28. Gordo O (2007) Why are bird migration dates shifting? A review of weather and climate effects on avian migratory phenology. *Climate Research* 35(1-2):37–58.
29. Wilman H, et al. (2014) EltonTraits 1.0: Species-level foraging attributes of the world's birds and mammals. *Ecology* 95(7):2027.
30. Herbers JR, Serrouya R, Maxcy KA (2004) Effects of elevation and forest cover on winter birds in mature forest ecosystems of southern British Columbia. *Can J Zool* 82(11):1720–1730.
31. Hannachi A, Jolliffe IT, Stephenson DB (2007) Empirical orthogonal functions and related techniques in atmospheric science: A review. *International Journal of Climatology* 27(9):1119–1152.
32. BirdLife International and NatureServe (2012) *Bird Species Distribution Maps of the World* (BirdLife International, Cambridge, UK and NatureServe, Arlington, VA).
33. Dawson W, Carey C (1976) Seasonal acclimatization to temperature in cardueline finches. *J Comp Physiol* 112(3):317–333.
34. Henttonen H, Kanninen M, Nygren M, Ojansuu R (1986) The maturation of *Pinus sylvestris* seeds in relation to temperature climate in Northern Finland. *Scandinavian Journal of Forest Research* 1(1-4):243–249.
35. Philipson JJ (1997) Predicting cone crop potential in conifers by assessment of developing cone buds and cones. *Forestry* 70(1):87–96.
36. Pukkala T, Hokkanen T, Nikkanen T (2011) Prediction models for the annual seed crop of Norway spruce and Scots pine in Finland. *Silva Fennica* 44:629–642.
37. Roland CA, Schmidt JH, Johnstone JF (2014) Climate sensitivity of reproduction in a mast-seeding boreal conifer across its distributional range from lowland to treeline forests. *Oecologia* 174(3):665–677.
38. Satake A, Iwasa Y (2000) Pollen coupling of forest trees: Forming synchronized and periodic reproduction out of chaos. *J Theor Biol* 203(2):63–84.
39. Draper NR, Smith H (1998) *Applied Regression Analysis* (Wiley-Interscience, Hoboken, NJ).
40. Smith FR (1959) The crossbill invasion of 1956 and the subsequent breeding in 1957. *British Birds* 52(1):1–9.
41. Ostfeld RS, Keesing F (2000) Pulsed resources and community dynamics of consumers in terrestrial ecosystems. *Trends Ecol Evol* 15(6):232–237.
42. Yang LH (2004) Periodical cicadas as resource pulses in North American forests. *Science* 306(5701):1565–1567.
43. Farrell SL, Morrison ML, Campomizzi AJ, Wilkins RN (2012) Conspecific cues and breeding habitat selection in an endangered woodland warbler. *J Anim Ecol* 81(5):1056–1064.
44. Crone EE, McIntire EJB, Brodie J (2011) What defines mast seeding? Spatio-temporal patterns of cone production by whitebark pine. *J Ecol* 99(2):438–444.
45. Jutla AS, Small D, Islam S (2006) A precipitation dipole in eastern North America. *Geophys Res Lett* 33(21):L21703.
46. Trenberth K, Hurrell J (1994) Decadal atmosphere-ocean variations in the Pacific. *Clim Dyn* 9(6):303–319.
47. Yu B, Wang XL, Zhang XB, Cole J, Feng Y (2013) Decadal covariability of the northern wintertime land surface temperature and atmospheric circulation. *J Clim* 27(2):633–651.
48. Kenyon J, Hegerl GC (2008) Influence of modes of climate variability on global temperature extremes. *J Clim* 21(15):3872–3889.
49. Lau KM, Weng H (2002) Recurrent teleconnection patterns linking summertime precipitation variability over east Asia and North America. *Journal of the Meteorological Society of Japan Series II* 80(6):1309–1324.
50. Schubert S, Wang H, Suarez M (2011) Warm season subseasonal variability and climate extremes in the Northern Hemisphere: The role of stationary Rossby waves. *J Clim* 24(18):4773–4792.
51. Han JP, Liu G, Xin YF (2014) A dipole pattern of summer precipitation over mid-high latitude Asia and related snow cover anomalies in the preceding spring. *Atmospheric and Oceanic Letters* 7(4):364–368.
52. Wells JV, ed (2011) Boreal birds of North America: A hemispheric view of their conservation links and significance. *Studies Avian Biol* (University of California Press, Berkeley, CA) Vol 41, pp 1–160.
53. Gao Y, et al. (2014) Robust spring drying in the southwestern U.S. and seasonal migration of wet/dry patterns in a warmer climate. *Geophys Res Lett* 41(5):1745–1751.
54. Shepard D (1968) A two-dimensional interpolation function for irregularly-spaced data. *Proceedings of the 1968 23rd Association for Computing Machinery National Conference* (ACM, New York), pp 517–524.
55. Hannachi A, Jolliffe IT, Stephenson DB (2007) Empirical orthogonal functions and related techniques in atmospheric science: A review. *J Clim* 27(9):1119–1152.
56. Thompson DWJ, Wallace JM (2000) Annular modes in the extratropical circulation. Part I: Month to month variability. *J Clim* 13(5):1000–1016.
57. Schneider U, et al. (2014) GPCC's new land surface precipitation climatology based on quality-controlled in situ data and its role in quantifying the global water cycle. *Theoretical and Applied Climatology* 115(1-2):15–40.
58. Dee DP, et al. (2011) The ERA-Interim reanalysis: Configuration and performance of the data assimilation system. *Quarterly Journal of the Royal Meteorological Society* 137(656):553–597.
59. Brandt P, et al. (2011) Interannual atmospheric variability forced by the deep equatorial Atlantic Ocean. *Nature* 473(7348):497–500.
60. Fenneman NM, Johnson DW (1946) *Physiographic Divisions of the Conterminous US* (US Geological Survey, Reston, VA).